

# Learning 6-D compliant motion primitives from demonstration

Markku Suomalainen and Ville Kyrki<sup>†</sup>

December 15, 2024

## Abstract

We present a novel method for learning 6-D compliant motions from demonstration. The key advantage of our learning method compared to current Learning from Demonstration (LfD) methods is that we learn to take advantage of existing mechanical gradients (such as chamfers) with compliance to perform in-contact motions consisting of both translation and rotation, as in aligning workpieces or attaching hose couplers. We find the desired direction, which leads the robot’s end-effector to the location shown in the demonstration either in free space or in contact, separately for translational and rotational motions. The key idea is to first compute a set of directions which would result in the observed motion at each timestep during a demonstration. By taking an intersection over all such sets from a demonstration we find a single desired direction which can reproduce the demonstrated motion. Finding the number of compliant axes and their directions in both rotation and translation is based on the assumption that in the presence of a desired direction of motion, all other observed motion is caused by the contact force of the environment, signalling the need for compliance. We evaluate the method on a KUKA LWR4+ robot with test setups imitating typical tasks where a human would use compliance to cope with positional uncertainty. Results show that the method can successfully learn and reproduce compliant motions by taking advantage of the geometry of the task, therefore reducing the need for initial accuracy.

## 1 INTRODUCTION

Currently robotic assembly is mainly performed inside mass production factories, where the environment can be precisely modelled and controlled and the production batch sizes are high. However, many assembly tasks occur in smaller batches or completely outside factories. The ability to automate assembly for

---

<sup>\*</sup>This work was supported by Academy of Finland, decision 286580.

<sup>†</sup>M. Suomalainen and V. Kyrki are with School of Electrical Engineering, Aalto University, Finland `firstname.surname@aalto.fi`

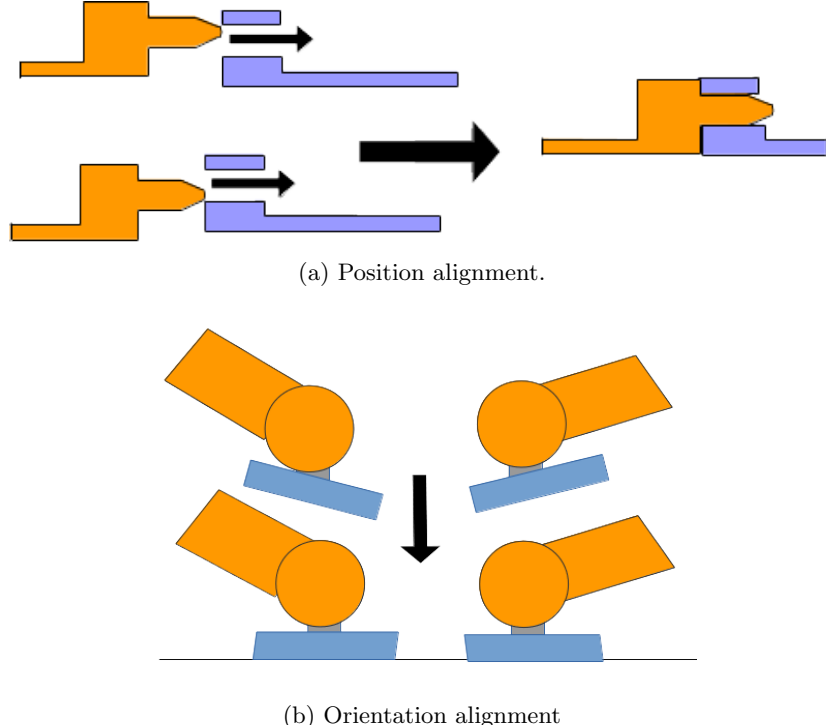


Figure 1: Compliant motions can be used for aligning both position and orientation of a workpiece

smaller product batches and tasks occurring outside factories has tremendous potential to increase the usage of robots worldwide.

Assembly motions can be difficult for robots since positional errors in tasks with small clearance often lead to high contact forces. It is essential that the contact wrenches (force and torque) are managed when interacting with the environment. Humans, on the other hand, can effectively take advantage of contact forces and utilize the arising compliant motions to mitigate positional uncertainty. A convenient control approach for compliant motions that does not require switching between different control strategies is impedance control [1], which features a virtual spring with adjustable stiffness between the tool and the environment. Impedance control allows small deviations from the desired trajectory, while still applying a stiffness-dependent wrench along the desired trajectory. This ability makes impedance controller a natural choice for performing compliant motions. Even though there has been a recent success in developing a feasible trajectory planner for 3-D compliant motions [2], there is need for end-user friendly learning methods for impedance-controlled compliant motions.

Learning from Demonstration (LfD) [3] is an established paradigm in robotics

for skill transfer and encoding. The key idea is that a human expert gives a demonstration of a task, which the robot then learns to reproduce. There are multiple methods for encoding the learned skill, such as Dynamic Movement Primitives (DMP) [4] and Gaussian Mixture Models (GMM) with Gaussian Mixture Regression (GMR) [5]. The main drawback of these methods for in-contact tasks is the tight coupling between force and position trajectories, which makes them susceptible to errors in initial position especially when dealing with multiple demonstrations. Even though recent publications have shown that with certain modifications DMPs can be used to realize unseen trajectories [6], a primitive without the force-position coupling would be more flexible for easy generalization to tasks similar to demonstration.

The method in this paper detects the complete 6-D desired direction of a motion, including both translation and rotation, and the required compliant axes in both translation and rotation as well. The desired direction is defined as a linear direction which, either through free space or with the help of a mechanical gradient such as a chamfer, leads the end-effector to the goal pose of the motion. We use kinesthetic teaching to show the robot an example of a motion. This work is an extension of our previous work [7], where the orientation was considered to be already aligned and remained fixed throughout the motion. The key difference to existing LfD methods for in-contact tasks is that we do not couple the position trajectory with the force/impedance profile. This renders our method more robust against positional and orientational errors.

The novelty in this paper includes: i) detecting if either translations or rotations are fully compliant due to work done by the environment and ii) modifying the computation of desired direction to work with rotational motions, evaluating if the desired direction is reliable and finding the compliant axes even when the desired direction is unreliable and iii) showing that the primitive can successfully learn to imitate a wide range of motions which can consist of both rotation and translation and require compliance along any direction or orientation. Learning the segmenting and sequencing of the primitives to complete a full task is outside of the scope of this paper.

## 2 RELATED WORK

The idea of using force control to take advantage of geometry in an assembly task is well established. Schimmels and Peshkin [8] defined already in 1991 the concept of geometric force-assemblability in 2-D using screw-theoretical concepts. Even earlier, Ohwovorile and Roth [9] used the concept of virtual work (defined as the dot product between the motion twist and the contact wrench) to divide twists into repelling, reciprocal or contrary. Their research inspired us to look into whether work is done by the human teacher or the environment, which is a key point when discovering whether all translational or rotational degrees of freedom must be compliant. Stolt [10] studied robotic assembly using high-level task specification and alternating position and force control. However, we believe that LfD provides an easier interface for the end-user to teach a task.

Moreover, impedance control does not require switching controllers between free space and in-contact motions, and therefore we believe it is more suitable for compliant assembly motions.

Learning workpiece alignment from demonstrations using DMP's has been presented by Peternel et al. [11], Abu-Dakka et al. [6, 12] and Kramberger et al. [13, 14]. Peternel et al. used an external interface for the teacher to manually modulate the required stiffness. Abu-Dakka et al. added a force feedback controller in the DMP's [6] and recently an impedance profile to GMM's [12]. Kramberger et al. performed a peg-in-hole task with varying hole depths, and also performed rotational motions. However, the tight coupling of position and force/impedance profiles makes the methods susceptible to positional errors at initial contact or demonstrations of different lengths. In contrast, the method presented in this paper can naturally learn from demonstrations of different length, and for generalization does not require information such as hole depth as used in [14].

There have been a few other recent publications about new LfD primitives to replace the aforementioned DMP and GMM/GMR strategies. Reiner et al. [15] and Rozo et al. [16] took advantage of the variations in the recorded trajectory to define where positional accuracy is important and therefore high stiffness required. However, their work was aimed towards free space motion and included the whole variance of demonstrations, whereas we look at the variance of motion outside a specified desired direction in an in-contact task. Ahmadzedah et al. [17] proposed an LfD encoding method which can generate unseen trajectories within the cylinder of the given demonstrations. However, both of these methods are presented as tools for free space motion and not for in-contact tasks. Racca et al. [18] used Hidden Semi-Markov Models (HSMM) with GMR to allow the teaching of in-contact tasks. However, even their work cannot take advantage of the task's geometry. Suomalainen and Kyrki [7] presented a compliant primitive that can take advantage of the task's geometry, but cannot perform rotational compliant motions or align the tool's orientation. This paper generalizes their method to work in 6-D and perform rotational motions as well.

### 3 METHOD

We assume that an assembly task can be divided into motion segments which can be completed with combinations of linear motion and compliance, using a method such as in [19, 20]. To complete the task, each segment can be executed with an impedance controller defined for the end-effector as

$$\begin{aligned}\mathbf{F} &= K_f(\mathbf{x}^* - \mathbf{x}) + D_f \mathbf{v} \\ \mathbf{T} &= K_o(\boldsymbol{\beta}^* - \boldsymbol{\beta}) + D_o \boldsymbol{\omega}\end{aligned}\tag{1}$$

where  $F, T$  are the force and torque used to control the robot,  $\mathbf{x}^*$  the desired position,  $\mathbf{x}$  the current position,  $\boldsymbol{\beta}^*$  the desired orientation,  $\boldsymbol{\beta}$  the current orientation,  $K_f$  and  $K_o$  stiffness matrices and  $D_f \mathbf{v}$  and  $D_o \boldsymbol{\omega}$  linear damping terms.

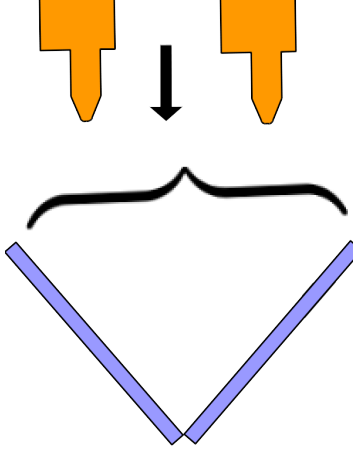


Figure 2: Illustration of the theoretical convergence region (black brace) of the algorithm in a pure translational case (similar as the "valley" experiment in [7]).

As each segment consists of an impedance controller primitive, we calculate the trajectory for each segment in a feed-forward manner

$$\begin{aligned} \mathbf{x}_t^* &= \mathbf{x}_{t-1}^* + \nu \Delta t \hat{\mathbf{v}}_d^* \\ \boldsymbol{\beta}_t^* &= \boldsymbol{\beta}_{t-1}^* + \lambda \Delta t \hat{\boldsymbol{\omega}}_d^* \end{aligned} \quad (2)$$

where  $\hat{\mathbf{v}}_d^*$  and  $\hat{\boldsymbol{\omega}}_d^*$  are the desired directions in translation and rotation,  $\Delta t$  the sample time of the control loop and  $\nu$  and  $\lambda$  the translational and rotational speeds. Throughout this paper, we will use the circumflex ( $\hat{\cdot}$ ) notation to denote the normalization of a vector (i.e.  $\hat{\mathbf{x}} = \frac{\mathbf{x}}{\|\mathbf{x}\|}$ ). Assuming that the damping is sufficient for stabilizing the dynamics, we propose a method to learn  $K_f$ ,  $K_o$ ,  $\hat{\mathbf{v}}_d^*$  and  $\hat{\boldsymbol{\omega}}_d^*$  separately for each primitive from one or more human demonstrations. In cases such as depicted in Figs. 1a or 1b, giving at least one demonstration from each shown starting position allows the algorithm to learn one set of parameters which can reproduce all motions from within the workpiece's zone of convergence (visualized for translation in Fig. 2).

A flowchart describing the whole process of learning  $K_f$ ,  $K_o$ ,  $\hat{\mathbf{v}}_d^*$  and  $\hat{\boldsymbol{\omega}}_d^*$  from a demonstrated motion is shown in Fig. 4. In Section 3.1 we validate whether the teacher performed only translation, i.e.  $\hat{\boldsymbol{\omega}}_d^*$  is zero (does not exist) even though rotation was observed. This results in all rotational degrees of freedom to be compliant, or vice versa if the teacher performs rotation only (called 3-DOF compliance in this paper). If this is not observed, in Section 3.2 the algorithm checks whether  $\hat{\mathbf{v}}_d^*$  or  $\hat{\boldsymbol{\omega}}_d^*$  or both exist. Finally, in Section 3.3 it is evaluated if individual degrees of freedom are required to be compliant, yielding  $K_f$  and  $K_o$ . As an end result, there can be a desired direction in both translation and rotation, or in only one of them. In addition, compliance is found for both rotation and translation, if required.

The method requires that during the demonstration, a force/torque (F/T)

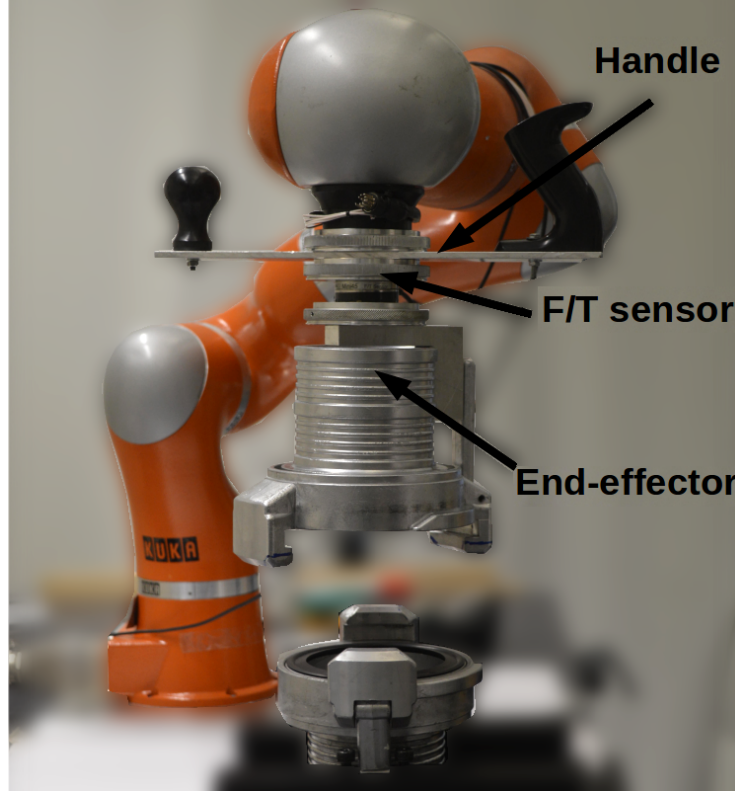


Figure 3: The KUKA LWR4+ robot used for the experiments, with equipment for the hose coupler setup attached.

sensor is placed between the tool and the place where the teacher grabs the robot, such as in Fig. 3. Wrench and pose (position and orientation) data at the F/T sensor are recorded, and the force measured by the F/T sensor during contact (neglecting Coriolis and centrifugal force) can be written as

$$\mathbf{F}_m = \mathbf{F}_N + \mathbf{F}_\mu + m\mathbf{a} \quad (3)$$

where  $\mathbf{F}_m$  is the force measured by the F/T sensor,  $\mathbf{F}_N$  the normal force,  $\mathbf{F}_\mu = |\mu\mathbf{F}_N|(-\hat{\mathbf{v}}_a)$  the force caused by Coulomb friction with  $\mu$  being the friction coefficient and  $\hat{\mathbf{v}}_a$  the actual direction of motion,  $m$  the mass of the tool and  $\mathbf{a}$  its acceleration. Similarly, the measured torque  $\mathbf{T}_m$  can be written as

$$\mathbf{T}_m = \boldsymbol{\rho} \times \mathbf{F}_N + \mathbf{l} \times \mathbf{F}_\mu + I\boldsymbol{\alpha} \quad (4)$$

where  $\mathbf{l}$  and  $\boldsymbol{\rho}$  are the lever arm position vectors perpendicular to corresponding applied forces,  $I$  the inertia matrix and  $\boldsymbol{\alpha}$  the angular acceleration. Although this model is for a single-point contact, we show that the method is robust enough that we can teach multi-point contact tasks as well; considering a thorough contact formation treatment is outside the scope of this paper. We assume

that the speed of the end-effector is close to constant and therefore the acceleration terms can be ignored from both equations.

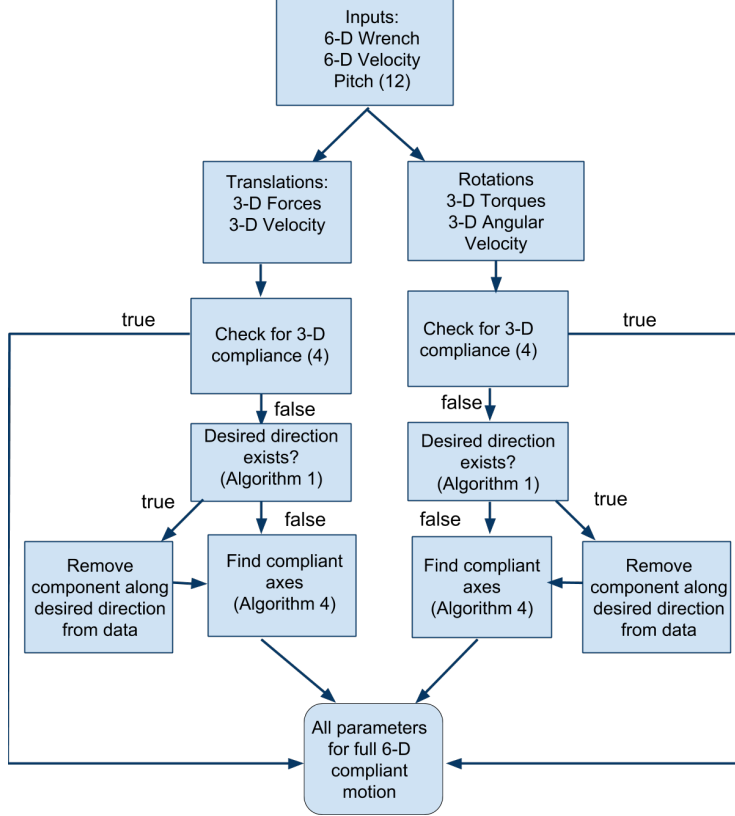


Figure 4: A flowchart describing the whole process of finding the 6-D compliant primitive to reproduce a demonstrated motion.

### 3.1 Checking for 3-DOF compliance

In 6-D motion it is possible that, due to contact forces, translational force applied by the teacher causes rotation, or vice versa. In such a case, either the observed translation or rotation is caused completely by the environment and the corresponding degrees of freedom need to be set compliant (i.e. 3-DOF compliance). More insight into the kind of motion falling into this category can be found from Fig. 7 and Section 4.2.

The intuition to detect this phenomenon stems from the definition of work in physics, which is defined for translational and rotational motions as

$$\begin{aligned} W_x &= \mathbf{F}_m \cdot \Delta \mathbf{x} \\ W_\beta &= \mathbf{T}_m \cdot \Delta \beta \end{aligned} \tag{5}$$

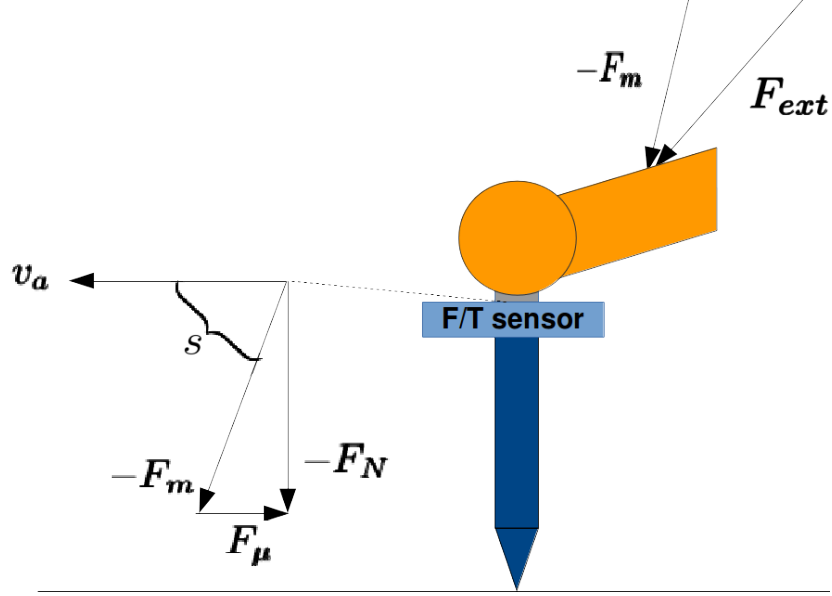


Figure 5: Force/torque sensor configuration, the position where external wrench by the human teacher  $\mathbf{F}_{ext}$  is applied and the forces which sum up to the reading of the force measurement  $\mathbf{F}_m$  of the F/T sensor.

where  $W$  is the work,  $\Delta\mathbf{x}$  the change in translation and  $\Delta\beta$  the change in angle. If the majority of work is done by the environment, we assume that those degrees of freedom (all rotational or translational degrees of freedom) should be compliant since the demonstrator was not explicitly performing those motions but they were caused by the environment. Formally, either rotation or translation is 3-DOF compliant if

$$\frac{W_{env}}{W_{tot}} \geq \sigma \quad (6)$$

where  $W_{tot}$  is the total work during a demonstration and  $W_{env}$  the work done by the environment. We can compute  $W_{tot}$  by

$$W_{tot} = \int |W| dt \quad (7)$$

where  $W$  is either  $W_x$  or  $W_\beta$  and taking the absolute value means that we consider work to be path-dependent. As the wrench measured by the F/T sensor is the contact wrench, i.e. caused by the environment, work performed by the environment is observed as positive values for  $W$ . Therefore we can compute  $W_{env}$  as

$$W_{env} = \int W_+ dt, \quad W_+ = \begin{cases} W & \text{if } W > 0 \\ 0 & \text{else} \end{cases} \quad (8)$$

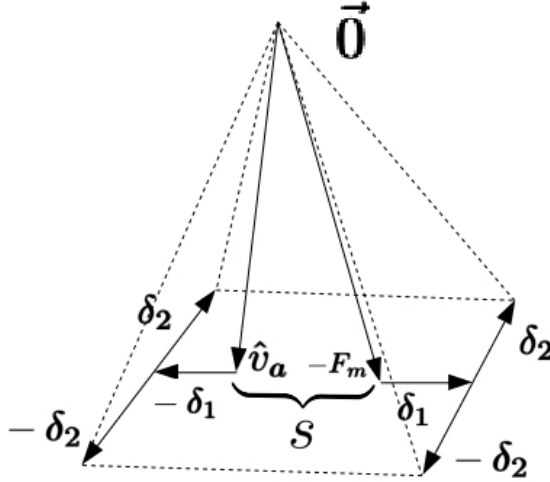


Figure 6: Illustration of expanding 2-D sector  $s$  for translations into 3-D set of directions  $P$  in (9) and (10). Continuous lines represent the vectors and dotted lines highlight the pyramid shape.

The choice of  $\sigma$  in (6) depends on the task and the accuracy of demonstration; with perfect demonstrations  $\sigma$  could be set to 1, but in practice it has to be reduced to allow human inconsistencies during a demonstration. If the ratio is below  $\sigma$ , Algorithm 1 is run as described in Fig. 4 and in the next section. Otherwise rotation or translation is set to 3-DOF compliant.

### 3.2 Learning desired direction

In this section we describe the method to learn  $\hat{v}_d^*$  and  $\hat{\omega}_d^*$ . To slide the robot’s tool in contact, the robot can be pushed from any direction from the sector  $s$  defined as the 2-D sector between the actual direction of motion  $v_a$  and the force measured by the F/T sensor  $F_m$ , as seen in (3) and Fig. 5. Our key idea is to extend this insight into rotations and 3-D such that at each measurement point of a demonstration, we find a set of force and torque directions which would result in the observed direction of motion. By taking an intersection over many such sets, we can reproduce motions which can be represented with linear impedance controller parameters. The same algorithm is used to find both  $\hat{v}_d^*$  and  $\hat{\omega}_d^*$ .

To find an intersection of sectors over a real demonstration in 3-D, sector  $s$  must be expanded since a human cannot perform a perfect demonstration (for example, sliding along a straight line on a surface). We expand the sector both perpendicular to  $s$  and along the direction of  $s$ , as seen in Fig. 6.

Formally, we define the vectors extending the sector  $s$  at each time step  $t$  as

$$\begin{aligned}\boldsymbol{\delta}_{1,t} &= \tan \xi \frac{-\widehat{\Pi}_t - \widehat{\psi}_{a,t}}{|\widehat{\Pi}_t - \widehat{\psi}_{a,t}|} \\ \boldsymbol{\delta}_{2,t} &= \tan \eta \frac{-\widehat{\Pi}_t \times \widehat{\psi}_{a,t}}{|\widehat{\Pi}_t \times \widehat{\psi}_{a,t}|}\end{aligned}\quad (9)$$

where  $(\widehat{\Pi}, \widehat{\psi}) \in \{(\widehat{F}_m, \widehat{v}), (\widehat{T}_m, \widehat{\omega})\}$ , i.e.  $\widehat{\Pi}$  and  $\widehat{\psi}$  represent either forces and translational motions or torques and rotational motions. Throughout this paper the subscript  $d$  refers to “desired” direction and  $a$  to “actual”, the latter meaning the observed direction of motion, either translation or rotation. Variable  $\eta$  is the angle with which we wish to extend the sector  $s$  perpendicularly and  $\xi$  the angle used to widen the sector. Thus the limits of a desired direction of motion, as illustrated in Fig. 6 for translations, at each time step  $t$  can be written as a set of vectors

$$P_t = \left\{ \widehat{\psi}_{d,t} - \boldsymbol{\delta}_{1,t} + \boldsymbol{\delta}_{2,t}, \widehat{\psi}_{d,t} - \boldsymbol{\delta}_{1,t} - \boldsymbol{\delta}_{2,t}, -\widehat{\Pi}_t + \boldsymbol{\delta}_{1,t} + \boldsymbol{\delta}_{2,t}, -\widehat{\Pi}_t + \boldsymbol{\delta}_{1,t} - \boldsymbol{\delta}_{2,t} \right\} \quad (10)$$

where  $P_t$  represents the set of vectors limiting the desired directions of motion  $\widehat{\psi}_{d,t}$  at a single time step  $t$  in 3-D, either translational or rotational. Thus we can write the range of possible desired directions at time step  $t$  as a positive linear combination of the vectors in  $P_t$ , as

$$\widehat{\psi}_{d,t} = \left| \sum w_i \mathbf{p}_i \right| \quad (11)$$

where  $w_i \geq 0$  and  $\mathbf{p}_i \in P_t$ . All  $P_t$  over one or more demonstrations are then projected into 2-D rectangles  $\Theta_t$  over a demonstration and  $\widehat{\mathbf{v}}_d^*$  and  $\widehat{\mathbf{\omega}}_d^*$  are chosen as the Chebyshev center [21] of the intersection of rectangles  $\Theta_t$ . The whole algorithm is formulated in Algorithm 1, where computation of each  $P_t$  is shown on line 3.

To avoid problems due to representation of orientation, the data is rotated on lines 1 and 5 in Algorithm 1. Then, to facilitate the computations, each 3-D data point is projected into 2-D unit circle using function **vec2ang** described in Algorithm 2. On lines 9-15 in Algorithm 1 outlier rejection is performed: we find, on a chosen scale, the point  $(i, j)$  of grid  $G$  which is enclosed by the maximum number of rectangles  $\Theta_t$ . Then on lines 16-21 we choose from the set of rectangles  $\Theta$  the subset  $\Theta^*$  which include the point  $(i, j)$ . Then we compute the intersection  $\Phi$  of rectangles  $\Theta^*$ , compute the Chebyshev center  $\boldsymbol{\phi}^*$  of  $\Phi$ , convert  $\boldsymbol{\phi}^*$  back to a 3-D vector with function **ang2vec** (Algorithm 3) and rotate it back to get  $\widehat{\psi}_d^*$ . The process is similar to [7], where it is explained in more detail.

Since a motion can consist of both translation and rotation, it is possible that for either translation or rotation there does not exist a desired direction, even if 3-DOF compliance is not detected in (6). This can be evaluated from the

---

**Algorithm 1** Computation of desired direction

---

**Input:** Sets  $\Psi, \Pi$  consisting of  $\hat{\psi}_{a,t}, \hat{\Pi}_t$ .  
**Output:** Desired direction  $\hat{\psi}_d^*$ .

- 1: Determine  $R$  that rotates mean  $\bar{\psi}_a$  of all  $\hat{\psi}_{a,t}$  to positive z axis
- 2: **for** each measurement point  $t$  **do**
- 3:     Calculate  $P_t$  from  $\hat{\psi}_{a,t}, \hat{\Pi}_t$  (9),(10)
- 4:     **for** each  $\mathbf{p}_i$  in  $P_t$  **do**
- 5:          $\Theta_t = \Theta_t \cup \text{vec2ang}(R\mathbf{p}_i)$
- 6:     **end for**
- 7:      $\Theta = \Theta \cup \Theta_t$
- 8: **end for**
- 9:  $G(i, j) = 0 \forall i, j$
- 10: **for** each  $\Theta_t \in \Theta$  **do**
- 11:     **for**  $(i, j)$  inside rectangle formed by  $\Theta_t$  **do**
- 12:          $G(i, j) = G(i, j) + 1$
- 13:     **end for**
- 14: **end for**
- 15:  $(i, j)_{max} = \arg \max_g \forall g_{i,j}$  in  $G$
- 16: **for** each  $\Theta_t$  in  $\Theta$  **do**
- 17:     **if**  $(i, j)_{max}$  inside  $\Theta_t$  **then**
- 18:          $\Theta^* = \Theta^* \cup \Theta_t$
- 19:     **end if**
- 20: **end for**
- 21:  $\Phi = \bigcap_t \Theta_t^*$
- 22: Calculate Chebyshev center  $\phi^*$  of  $\Phi$
- 23:  $\hat{\psi}_d^* = R^{-1} \text{ang2vec}(\phi^*)$

---

---

**Algorithm 2**  $\text{vec2ang}()$ .

---

**Input:** Cartesian 3-D vector  $\mathbf{p}$ .  
**Output:** Angular 2-D vector  $\theta$ .

- 1:  $\hat{\mathbf{p}} = \frac{\mathbf{p}}{|\mathbf{p}|}$
- 2:  $r = \arccos(\hat{p}_z)$
- 3:  $\gamma = \arctan 2(\hat{p}_y, \hat{p}_x)$
- 4:  $\theta_x = r \cos(\gamma)$
- 5:  $\theta_y = r \sin(\gamma)$

---

---

**Algorithm 3** ang2vec().

---

**Input:** Angular 2-D vector  $\theta$ .  
**Output:** Cartesian 3-D vector  $p$ .  
1:  $S = \text{sign}(\arctan 2(\theta_y, \theta_x))$   
2:  $r = \cos(\sqrt{\theta_x^2 + \theta_y^2})$   
3:  $a = \frac{\theta_y}{\theta_x}$   
4:  $\hat{p}_z = \arccos(r)$   
5:  $\hat{p}_x = S \sqrt{\frac{1 - \hat{p}_z^2}{1 + a^2}}$   
6:  $\hat{p}_y = S a \hat{p}_x$

---

ratio of outliers i.e. the ratio between the number of rectangles in the set that contributed to the computation of  $\Phi$ ,  $\Theta^*$ , and all the rectangles  $\Theta$ . If this ratio is low, it means that there has been a large number of outliers and therefore the corresponding  $\hat{\psi}_d^*$  is unreliable. Formally, we assume there is no desired direction if

$$\frac{|\Theta^*|}{|\Theta|} < \zeta \quad (12)$$

where  $\zeta$  is a threshold for the ratio and  $|\cdot|$  denotes the cardinality of a set, i.e. the number of elements in it. The value of  $\zeta$  depends on the number and type of demonstrations. If, for example, two demonstrations are given from opposite sides such as in Fig. 1a, the value of  $\zeta$  should be over 0.5 to ensure that there exists a common desired direction for the two demonstrations. If the ratio for either translations or rotations is below  $\zeta$ , then there is no motion in those degrees of freedom. Whether compliance is required along particular axes is tested as described in the next section, and the non-compliant axes will be set stiff.

Finally, if both  $\hat{\psi}_d^*$  and  $\hat{\omega}_d^*$  exist, the ratio between rotational and translational motion must be calculated from unnormalized data. Borrowing from screw theory, we call this value the pitch, defined as

$$\pi = \frac{d_x}{d_\beta} \quad (13)$$

where  $\pi$  is the pitch,  $d_x$  is the translational distance covered and  $d_\beta$  the rotational distance covered. Now  $\nu$  and  $\lambda$  must be set in (2) according to  $\pi$  such that  $\nu = \pi\lambda$ . We want to note the possibility that  $\hat{\psi}_d^*$  is found in a case where the task requires keeping either rotations or translations only stiff. In such a case the pitch  $\pi$  is important: it will make the velocity small enough that the motion in reproduction is minimal, essentially keeping those degrees of freedom stiff.

### 3.3 Learning axes of compliance

This section presents how to learn  $K_f$  and  $K_o$  such that, together with  $\hat{\mathbf{v}}_d^*$  and  $\hat{\omega}_d^*$ , the demonstrated motion can be reproduced. Our key assumption for detecting the axes of compliance is that if there is motion in other directions besides  $\hat{\psi}_d^*$ , that motion must be caused by the environment, signalling a direction where compliance is required. We assume that if compliance is required along an axis, it must be totally compliant (i.e. stiffness equals zero). Hence if  $\hat{\mathbf{v}}_d^*$  exists, the axes of compliance defined in  $K_f$  must be perpendicular to  $\hat{\mathbf{v}}_d^*$ , and similarly for  $\hat{\omega}_d^*$  and  $K_o$ . We find the directions of the compliant axes with the help of Principal Component Analysis (PCA). We compute likelihoods of how well each PCA vector fits the data and based on that decide which of the PCA vectors need to be compliant. The whole process for defining the compliant axes is presented in Algorithm 4.

---

**Algorithm 4** Finding the required number of compliant axes and their directions.

---

**Input:** Desired direction  $\hat{\psi}_d^*$ , matrix  $\bar{\Psi}_a$  consisting of mean directions  $\bar{\psi}_{a,j}$  from each  $j$  demonstration.

**Output:**  $D$  number of compliant axes and  $U_D$  their directions.

```

1: if  $\hat{\psi}_d^* \neq \emptyset$  then
2:   for  $\bar{\psi}_{a,j} \in \bar{\Psi}_a$  do
3:      $\bar{\psi}_{a,j} = \bar{\psi}_{a,j} - (\bar{\psi}_{a,j} \cdot \hat{\psi}_d^*) \hat{\psi}_d^*$ 
4:   end for
5: end if
6: for  $d = 0 \dots 3$  degrees of freedom do
7:    $U_d = \text{rank } d$  PCA approximation of  $\bar{\Psi}_a$ 
8:   for  $\bar{\psi}_{a,j}$  in  $\bar{\Psi}_a$  do
9:      $\epsilon_{d,j} = (I - U_d) \bar{\psi}_{a,j}$ 
10:    end for
11:    $L_d = \prod_j \mathcal{N}(\epsilon_{d,j} | \mathbf{0}, \Sigma)$ 
12:   Calculate  $BIC_d$  with  $L_d$ , (14)
13: end for
14:  $D = \arg \min_d BIC_d$ 

```

---

To enforce the orthogonality between  $\hat{\psi}_d^*$  and the axes of compliance when  $\hat{\psi}_d^*$  exists, we remove the component along  $\hat{\psi}_d^*$  from the mean of actual motion  $\bar{\psi}_a$  by the computation on line 3 in Algorithm 4. Now any non-zero values of  $\bar{\psi}_a$  correspond to motion outside the direction of  $\hat{\psi}_d^*$ .

Our idea is to validate how many degrees of freedom are required to explain  $\bar{\psi}_a$  by calculating the likelihoods  $L_d$  for each  $d$  number of compliant axes. These degrees of freedom can be understood roughly as the number of linear directions of motion caused by the environment. We use PCA to find the eigenvectors i.e. directions of maximum variance of the data such that they form an orthonormal

base. If  $\bar{\psi}_a \approx 0$ , then  $\bar{\psi}_a$  is best explained by the origin only, corresponding to  $U_d = U_0$  (i.e. a rank 0 matrix, meaning zero matrix) and meaning that no compliance is required. If one axis of compliance is required, all motion  $\bar{\psi}_a$  has been along a single line, the first principle component corresponding to rank 1 PCA approximation  $U_1$ . For two axes of compliance, the plane described by the first two principal components best explains the motions. Finally, if not even a plane can explain the data, we require all three axes to be compliant, which can only happen if there is no  $\hat{\psi}_d^*$ . These computations happen on rows 6-11 on Algorithm 4.

Since we wish to give preference to simpler models, for choosing the final  $D$  we take inspiration from Bayesian Information Criterion (BIC) [22], which is defined

$$BIC = \ln(n)k - 2\ln(L) \quad (14)$$

where  $n$  is the number of data points,  $k$  the number of parameters and  $L$  the likelihood of a model. Now we can choose the correct model on rows 12-14 on Algorithm 4.

It should be noted that the proposed approach does not follow the typical use of BIC which is only applicable when  $n \gg k$  and the variance in the likelihood is calculated from the data. Instead, we assume that the uncertainty of demonstrations can be estimated beforehand, making it possible to use the proposed formulation. Also, we note that although here the three axes of compliance outcome is the same as from (6) in Section 3.1, the mechanism behind these outcomes is different: without calculating (6) in Section 3.1, the method in Section 3.2 can detect a desired direction for translations in a case where the cause is actually rotation and the normal force of the environment, or vice versa. Therefore, these two methods are not overlapping.

If more than one demonstrations are given, the demonstrations are concatenated and the method works exactly the same way. The number of required demonstrations depends on the application and the quality of the demonstrations: with good demonstrations, no more than one demonstration from each approach direction is required. However, there is a lower bound: Algorithm 4 cannot detect more degrees of freedom than provided demonstrations. Therefore to take advantage of geometrical properties of the task such as in Fig. 1a and 1b, at least two demonstrations are required. It should also be noted that with only one demonstration, (14) is not applicable since the first term will always go to zero.

## 4 EXPERIMENTS AND RESULTS

We used a KUKA LWR4+ lightweight arm to test our method. The demonstrations were recorded in gravity compensation mode, where the robot's internal sensors recorded the pose of the robot and an ATI mini45 F/T sensor placed at the wrist of the robot recorded the wrench. We implemented our controller through the Fast Research Interface (FRI) [23], where the controller is defined

as

$$\boldsymbol{\tau} = J^T(\text{diag}(\mathbf{k}_{\mathbf{FRI}})(\mathbf{x}^* - \mathbf{x}) + \text{diag}(\mathbf{d}_{\mathbf{FRI}})\mathbf{v} + \mathbf{F}_{\mathbf{FRI}}) + \mathbf{f}_{\mathbf{dyn}} \quad (15)$$

where  $J$  is the Jacobian,  $\text{diag}(\mathbf{k}_{\mathbf{FRI}})$  a diagonal matrix constructed of the gain values of  $\mathbf{k}_{\mathbf{FRI}}$ ,  $\mathbf{x}^* - \mathbf{x}$  the difference between commanded and actual position and  $\boldsymbol{\tau}$  the commanded joint torques. We implemented our controller through the superposed Cartesian wrench term  $\mathbf{F}_{\mathbf{FRI}}$  (including both desired Cartesian force and torque) by setting  $\mathbf{k}_{\mathbf{FRI}} = \mathbf{0}$  and  $\mathbf{F}_{\mathbf{FRI}} = K(\mathbf{x}^* - \mathbf{x})$ , getting a controller equal to (1) where  $K$  is the stiffness matrix and the dynamics  $\mathbf{f}_{\mathbf{dyn}}$  and damping  $\text{diag}(\mathbf{d}_{\mathbf{FRI}})\mathbf{v}$  are managed by the KUKA's internal controller.

In practice, due to noise in the demonstration from human and measurement uncertainty, averaging over a chosen number of time steps to compute  $P$  in (10) produces more stable results. To filter the noise, we chose to average over 20 time steps of original 100Hz measuring frequency, which meant sampling  $P$  in 5Hz. We used manually estimated values of 20 degrees for  $\eta$  and 10 degrees for  $\xi$  in (9).

To evaluate the method for purely translational motion, we performed work-piece alignment on a similar valley setup as in [7] consisting of two aluminium plates set on 45 degrees angle with the table. The results are similar to [7] and not included here for brevity.

To evaluate the method for motions including rotation we performed four experiments, each of which includes teaching and reproduction. With the hose coupler shown in Fig. 3, we studied both the alignment phase with varying orientations as shown in Fig. 11 and the interlocking phase where the coupler is rotated to fix the parts together. With the peg-in-hole setup shown in Fig. 14, we analysed whether the method finds the correct parameters to slide the peg completely in when it starts from a wrong orientation but partly inside the hole. Finally, to study a case where rotations cause translations as explained in Section 3.1, we performed a motion where the peg is rotated around the edge of a table as shown in Fig. 7.

We used an end-effector coordinate system defined at the wrist of the robot (the F/T sensor) in the experiments. However, the choice of the most suitable coordinate system is task-dependent. Automatically choosing the coordinate system is outside the scope of this paper.

#### 4.1 Identification of desired direction of motion

Our goal was to study if 1) the inlier ratio check in (12) can correctly identify whether  $\hat{\omega}_d^*$  and  $\hat{v}_d^*$  are required and 2) if required,  $\hat{\omega}_d^*$  and  $\hat{v}_d^*$  computed with Algorithm 1 can reproduce the demonstrated motion. For this we used the peg-in-hole experiment setup, from which we recorded the angle between the peg and the plane as shown in 8. From every 5 degree angle between 5 and 35 degrees, we performed 5 demonstrations by grasping the robot and leading the peg to the hole.

A desired direction for translation was found for each angle approximately along the z-axis in tool coordinate system (Fig. 8). The robustness of identify-

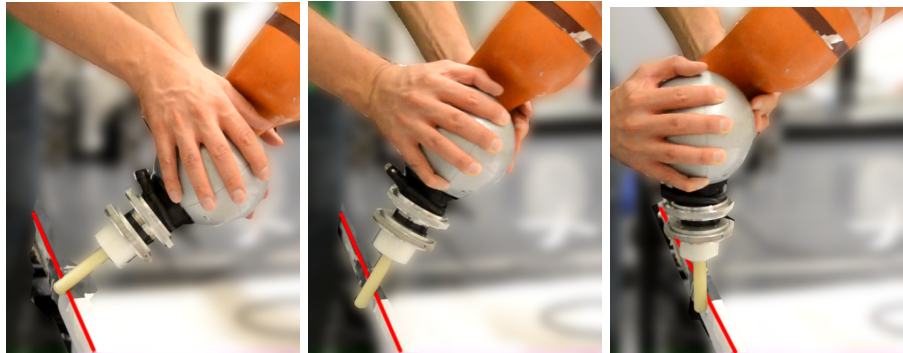


Figure 7: Screenshots from a demonstration of rotating the peg around the edge of the table, where the translational motion is caused by the contact forces. The edge of the table is highlighted in red.

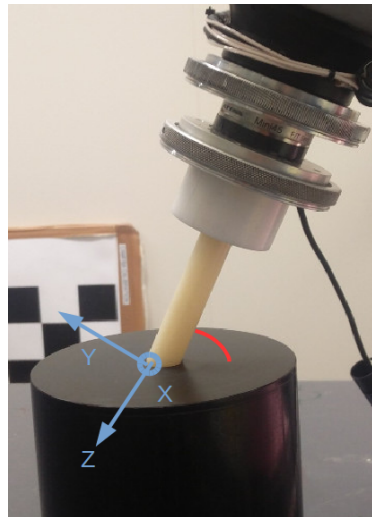


Figure 8: Illustration (in red) of the angle measured in Fig. 9. The tool coordinate system used in the experiments is shown in cyan.

ing translational desired direction was presented in [7]. For finding the desired direction for rotation, Fig. 9 shows 3 demonstrations with each starting angle of 5, 10, 15 and 20 degrees. It can be observed that the inlier ratio steadily increases with the increase of the starting angle. This corresponds to the fact that if the error angle (i.e. starting angle in this case, Fig. 8) is too large, a specific rotation needs to be introduced to complete the task. If, however, the error angle is low, it is enough to have compliance along the rotation along with a desired direction in translation. Our algorithm correctly captures this behaviour, and if the threshold  $\zeta$  was set to 0.6, as would be natural for three demonstrations,  $\hat{\omega}_d^*$  would exist when error angle is 15 degrees or more. Naturally the demonstrations are not required to be started from strictly the same error angle- combining demonstrations with error angle 10 or less degrees showed similar results, as did combining demonstrations with error angle of 15 degrees or more. When  $\hat{\omega}_d^*$  was required, the direction was correctly identified along the rotation.

To study the identification of the desired direction in the hose-coupler alignment, two demonstration from starting positions shown in Fig. 10b were given.  $\hat{v}_d^*$  was found but for the rotations, in Fig. 10b the inlier ratio was 0.41, leading us to conclude that there was no  $\hat{\omega}_d^*$ , therefore concluding that rotational compliance is enough to handle the kind of rotational alignment which was demonstrated. Also in the hose-coupler interlocking and peg-around-the-edge motions (Fig. 7)  $\hat{\psi}_d^*$  were correctly identified to replicate the motions. We conclude that our method can correctly identify the desired direction for both rotations and translations, and motion in both can be correctly combined to reproduce tasks such as peg-in-hole with high error angle, which requires both rotational and translational motions.

## 4.2 Learning axes of compliance

Our goal was to study whether our method can find the number of compliant axes and their directions in  $K_f$  and  $K_o$  which, together with the desired directions  $\hat{\omega}_d^*$  and  $\hat{v}_d^*$ , can reproduce the demonstrated motion. In the peg-around-the-edge motion (Fig. 7), the demonstration was performed such that the demonstrator was only rotating the tool, and the translation at the wrist occurred due to coupling of the translational and rotational motions. Therefore it was recognized in (6) that the translations need to be 3-DOF compliant. To give an insight about this result, the dot products between speed and force and between angular speed and torque are plotted over time in Fig. 12. It can be observed that with translations there is more work done by the environment than the demonstrator, since the curve stays on the positive semi-axis the whole time. The method correctly concluded that translations must be 3-DOF compliant in this motion.

In the other case where most of the work is not done by the environment, the number of compliant axes and their directions must be detected individually. The directions of the compliant axes are directly the vectors of the chosen matrix  $U_d$  from Algorithm 4. Vectors from  $U_3$  are visualized in Fig. 13 for the hose-

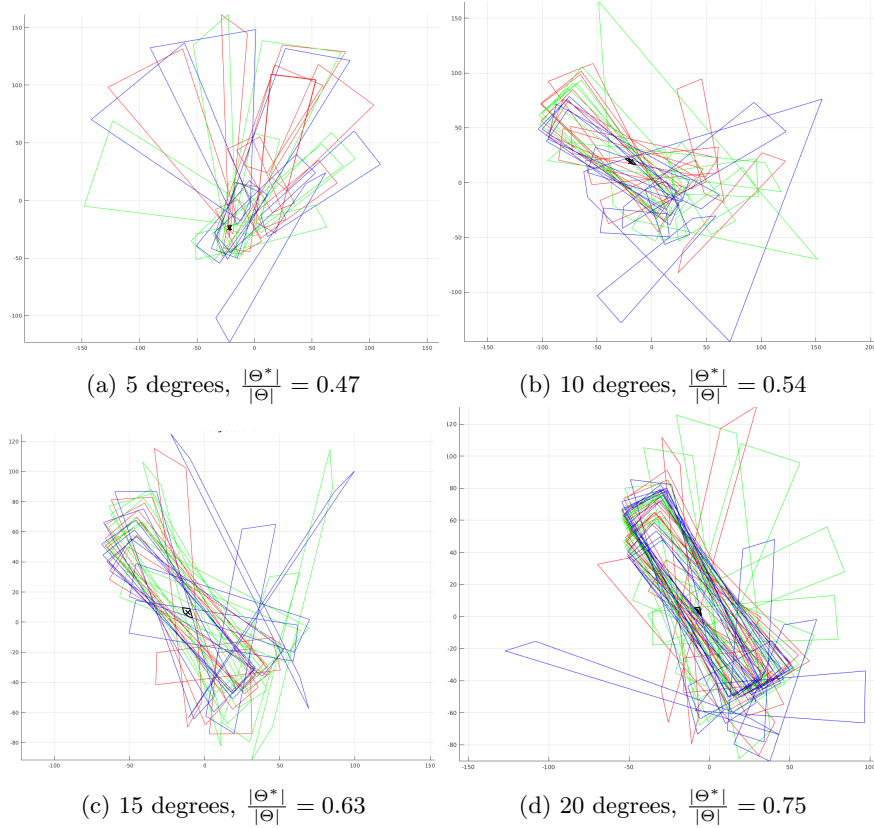
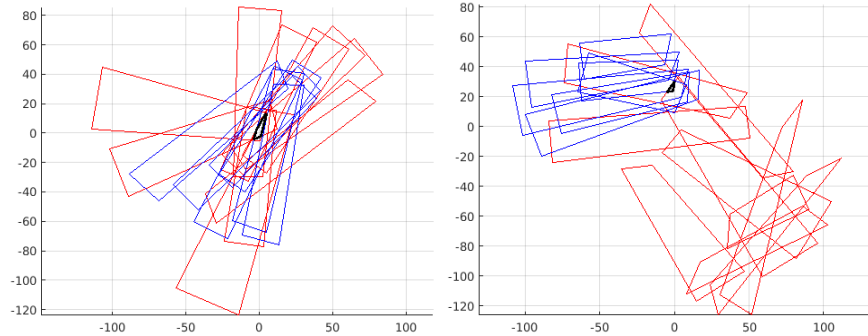


Figure 9: Visualization of lines 8-21 of Algorithm 1 to find the desired rotation direction for three demonstrations (each color corresponds to one demonstration) and the black rectangle is the intersection  $\Phi$ . Starting angles are 5-20 with respect to the hole and the corresponding inlier ratio  $\frac{|\Theta^*|}{|\Theta|}$  from (12) is shown below each subfigure.



(a) Hose-coupler alignment translations   (b) Hose-coupler alignment rotations

Figure 10: Visualization of lines 8-21 of Algorithm 1 to find the desired direction for either translations and rotations. The red and blue colors indicate the two separate demonstrations of the task and the black rectangle is the intersection  $\Phi$ , i.e. the set of all desired directions in the angle coordinate system.

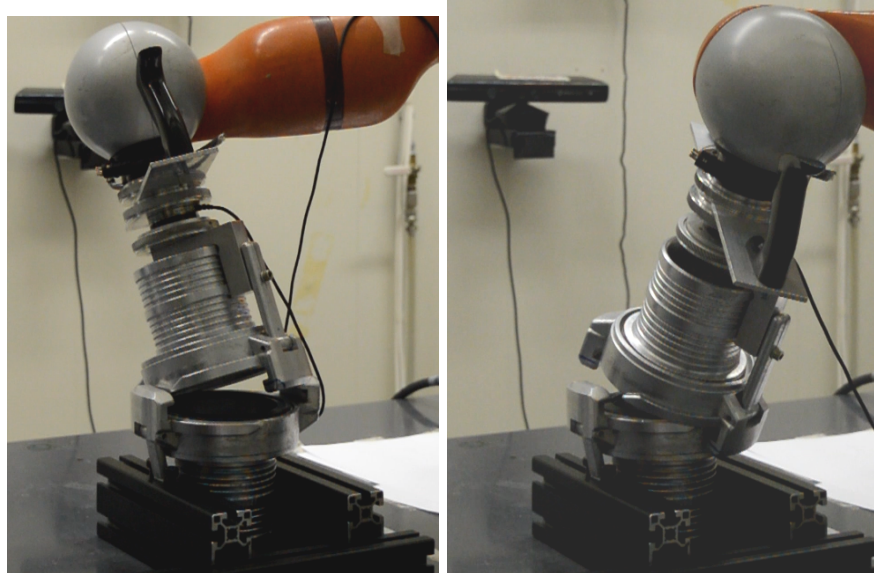


Figure 11: Two starting positions for demonstrations of the hose-coupler alignment task.

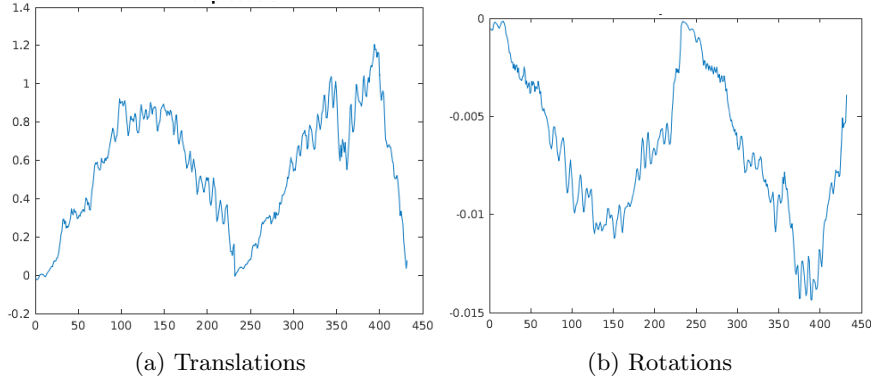


Figure 12: The dot products between speed and force and between angular speed and torque over time on the peg-around-the-edge motion.

coupler alignment task. It can be observed that the rotations are close to the origin, but still far enough that one compliant axis was detected, as required. When the component along  $\hat{v}_d^*$  is removed from  $\bar{v}_a$ , as in Fig. 13a, one axis of compliance ( $U_1$ ) is correctly identified, connecting the green crosses.

In the peg-in-hole experiments, at least one axis of compliance was detected for each error degree between 5 and 35. This is according to theory- without a desired direction, at least one compliant direction is required, whereas with a desired direction the compliant directions merely assist the motion. The difference is that whereas in 5-10 error degrees the first axis of compliance is found to approximately match the direction of motion, with higher error degrees the rotation motion is handled by  $\hat{\omega}_d^*$ . We conclude that the method correctly identified the compliant axes and their directions.

### 4.3 Reproduction of motion

Finally, to evaluate that the motions can be reproduced with the learned parameters, we performed the motions on all the aforementioned experiments. In [7] we already showed that the learning of desired direction is robust by randomizing over multiple sets of demonstrations. Now we show the interpolation and extrapolation capabilities in the peg-in-hole case- in particular, how much error can be tolerated with compliance alone, and when is actual rotation required.

In the peg-in-hole experiments, we first used parameters learned from all 5 demonstrations with 10 degrees of error. As shown in Fig. 9, no  $\hat{\omega}_d^*$  was found, but only  $\hat{v}_d^*$  along z-axis (Fig. 8 moves the peg. Compliance is required and found both in rotations and translations- in translations it is found along y-axis and in rotations around x-axis. With these parameters we performed five reproduction attempts starting from ever 5 degree angle. The peg is successfully inserted with error angles 5-15 degrees. With an error angle of 20 degrees, friction prevents sliding and the motion is unsuccessful.

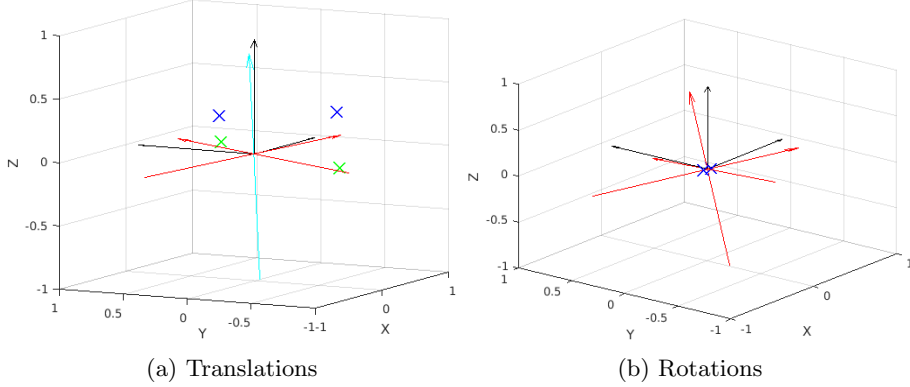


Figure 13: Illustrations of choosing the directions of compliant axes on the hose-coupler alignment experiment. The black arrows are coordinate axes, the red ones the eigenvectors  $U$  and the blue crosses the average motions of each demonstration,  $\psi_a$ . In (a)  $\hat{v}_d^*$  is plotted in cyan (overlapping the third eigenvector as expected) and the  $\bar{v}_a$  with the component along  $\hat{v}_d^*$  removed, as on line 3 in Algorithm 4, are plotted as green crosses. In both (a) and (b) 1 compliant axis is chosen

For the cases where both  $\hat{v}_d^*$  and  $\hat{\omega}_d^*$  were detected,  $\hat{v}_d^*$  was again along z-axis but  $\hat{\omega}_d^*$ , as expected, varied depending on the starting orientation of the tool. Nevertheless, for demonstrations recorded with 20 and 30 degrees error, reproduction was successful with the learned angle and lower angles but not on higher angles, signalling that the worst case should be demonstrated. These results are summarized in Table 1.

In Fig. 14 are shown screenshots from a reproduction of the P-I-H reproduction with 30 degrees error. Our algorithm also successfully reproduced the demonstrated motion on the hose-coupler alignment, hose-coupler interlocking and peg-around-the-edge experiments. We conclude that the parameters our method learns from human demonstration can be used to perform the motions

		Reproduction angle							
		5	10	15	20	25	30	35	
		10	✓	✓	✓	X	X	X	X
Demo angle		20	✓	✓	✓	✓	X	X	X
		30	✓	✓	✓	✓	✓	✓	X

Table 1: A table summing up the results of reproduction experiments. Each task was repeated 5 times, and the results were always failures only or successes only. Symbol **✓** marks success and **X** marks failure.

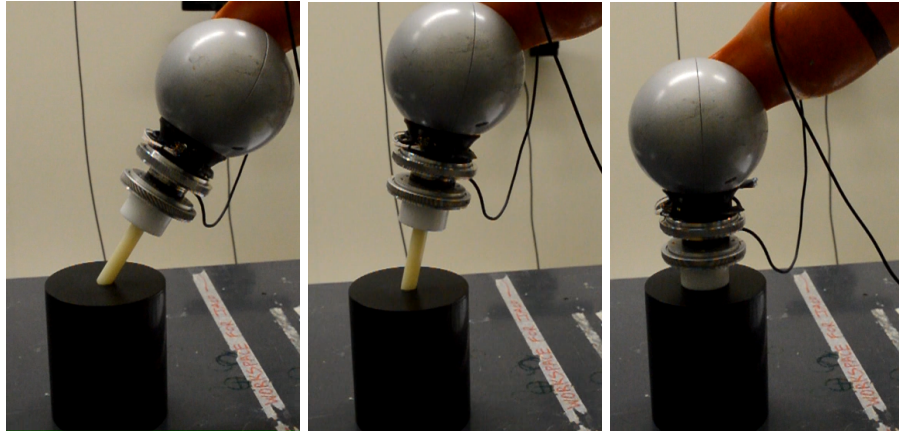


Figure 14: Screenshots from a reproduction video of the P-I-H motion. The motion starts from the leftmost picture, and the peg is rotated and pushed to the bottom. The peg has radius 16.5 mm, length 80 mm and a rounded tip, and the hole’s radius is 0.25 mm more than the peg’s.

with an impedance controller primitive.

## 5 CONCLUSIONS AND FUTURE WORK

We presented a method that can successfully learn and reproduce 6-D compliant motions from human demonstrations. The method finds a desired direction of motion which can be either pure translation, pure rotation or a combination of translation and rotation. Then it finds the compliant axes, both in translation and rotation, necessary to reproduce the motion. We found that compliance along rotation can compensate fairly significant errors in the angle. The exact angle depends heavily on the equipment, but in our setup the tolerance was fairly tight and a simple rounding of the tool’s end created enough of convergence region to take advantage of compliance. Advantages of using compliance only include the ability to use the same controller in free space, as demonstrated with translations in [7]. However, for cases where the angle is not due to error but due to instructions, we show that we can learn an active rotation as well.

The method presented in this paper models an assembly task as a sequence of linear directions and compliances. Physical modelling of the contact allows us to use intersection in the desired direction computations. Due to the use of intersection, it is easy to combine as many timesteps as required and thus the number of demonstrations or their ratio of lengths do not cause issues, in contrast to DMP which calculates the average over many demonstrations. Also since our method is programmed to perform the learned linear motion until physical constraints, our primitive generalizes to holes of different depth

and chamfers of different length. Finally, not following a pre-specified force trajectory but instead using compliance to adapt to new situations makes our method more robust towards errors in the initial position of the motion. On the other hand, DMP-based methods would perform better in tasks which require non-linear motions in free space or motions where the final position of the motion is not physically constrained.

A whole task would typically consist of a sequence of the primitives presented in this paper. Methods for sequencing primitives with linear dynamics is a common problem, for which various possible solutions have been presented [19, 20]. The method presented in this paper is meant mainly for assembly tasks in situations where the coordinate transformations between the robot and the target are not accurately known and the use of vision is complicated. Such a situation arises in, for example, in small-to-medium size enterprises, where a robot must be included in an existing working environment and CAD models of the workpieces are not available.

In [7] the world coordinate system was used, while in this work we chose the tool coordinate system. Both coordinate systems have their advantages and disadvantages and the choice is task-dependent. A method to automatically choose the most suitable coordinate system would enhance the method’s usability.

## References

- [1] N. Hogan, “Stable execution of contact tasks using impedance control,” in *Robotics and Automation. Proceedings. 1987 IEEE International Conference on*, vol. 4, pp. 1047–1054, IEEE, 1987.
- [2] C. Guan, W. Vega-Brown, and N. Roy, “Efficient planning for near-optimal compliant manipulation leveraging environmental contact,” in *Robotics and Automation (ICRA), 2018 IEEE International Conference on*. IEEE, 2018.
- [3] B. D. Argall, S. Chernova, M. Veloso, and B. Browning, “A survey of robot learning from demonstration,” *Robotics and autonomous systems*, vol. 57, no. 5, pp. 469–483, 2009.
- [4] S. Schaal, “Dynamic movement primitives-a framework for motor control in humans and humanoid robotics,” in *Adaptive Motion of Animals and Machines*, pp. 261–280, Springer, 2006.
- [5] S. Calinon, F. Guenter, and A. Billard, “On learning, representing, and generalizing a task in a humanoid robot,” *IEEE Transactions on Systems, Man, and Cybernetics, Part B (Cybernetics)*, vol. 37, no. 2, pp. 286–298, 2007.
- [6] F. J. Abu-Dakka, B. Nemec, J. A. Jørgensen, T. R. Savarimuthu, N. Krüger, and A. Ude, “Adaptation of manipulation skills in physical contact with the environment to reference force profiles,” *Autonomous Robots*, vol. 39, no. 2, pp. 199–217, 2015.

- [7] M. Suomalainen and V. Kyrki, “A geometric approach for learning compliant motions from demonstration,” in *Humanoid Robots (Humanoids), 2017 IEEE-RAS 17th International Conference on*, pp. 783–790, IEEE, 2017.
- [8] J. M. Schimmels and M. A. Peshkin, “Force-assemblability: Insertion of a workpiece into a fixture guided by contact forces alone,” in *Robotics and Automation, 1991. Proceedings., 1991 IEEE International Conference on*, pp. 1296–1301, IEEE, 1991.
- [9] M. Ohwovoriole and B. Roth, “An extension of screw theory,” *Journal of mechanical design*, vol. 103, no. 4, pp. 725–735, 1981.
- [10] A. Stolt, *On Robotic Assembly using Contact Force Control and Estimation*. PhD thesis, Lund University, 2015.
- [11] L. Peternel, T. Petrič, and J. Babič, “Human-in-the-loop approach for teaching robot assembly tasks using impedance control interface,” in *Robotics and Automation (ICRA), 2015 IEEE International Conference on*, pp. 1497–1502, IEEE, 2015.
- [12] F. J. Abu-Dakka, L. Rozo, and D. G. Caldwell, “Force-based variable impedance learning for robotic manipulation,” *Robotics and Autonomous Systems*, 2018.
- [13] A. Kramberger, A. Gams, B. Nemec, C. Schou, D. Chrysostomou, O. Madsen, and A. Ude, “Transfer of contact skills to new environmental conditions,” in *Humanoid Robots (Humanoids), 2016 IEEE-RAS 16th International Conference on*, pp. 668–675, IEEE, 2016.
- [14] A. Kramberger, A. Gams, B. Nemec, D. Chrysostomou, O. Madsen, and A. Ude, “Generalization of orientation trajectories and force-torque profiles for robotic assembly,” *Robotics and Autonomous Systems*, vol. 98, pp. 333–346, 2017.
- [15] B. Reiner, W. Ertel, H. Posenauer, and M. Schneider, “Lat: A simple learning from demonstration method,” in *Intelligent Robots and Systems (IROS 2014), 2014 IEEE/RSJ International Conference on*, pp. 4436–4441, IEEE, 2014.
- [16] L. Rozo Castañeda, S. Calinon, D. Caldwell, P. Jimenez Schlegl, and C. Torras, “Learning collaborative impedance-based robot behaviors,” in *Proceedings of the Twenty-Seventh AAAI Conference on Artificial Intelligence*, pp. 1422–1428, 2013.
- [17] S. R. Ahmadzadeh, M. A. Rana, and S. Chernova, “Generalized cylinders for learning, reproduction, generalization, and refinement of robot skills.,” in *Robotics: Science and Systems*, vol. 1, 2017.

- [18] M. Racca, J. Pajarinen, A. Montebelli, and V. Kyrki, “Learning in-contact control strategies from demonstration,” in *Intelligent Robots and Systems (IROS), 2016 IEEE/RSJ International Conference on*, pp. 688–695, IEEE, 2016.
- [19] O. Kroemer, H. Van Hoof, G. Neumann, and J. Peters, “Learning to predict phases of manipulation tasks as hidden states,” in *Robotics and Automation (ICRA), 2014 IEEE International Conference on*, pp. 4009–4014, IEEE, 2014.
- [20] T. Hagos, M. Suomalainen, and V. Kyrki, “Estimation of phases for compliant motions,” in *Intelligent Robots and Systems (IROS 2018), IEEE/RSJ International Conference on*, IEEE, 2018, Accepted for publication. arXiv:1809.00686.
- [21] A. L. Garkavi, “On the Chebyshev center and convex hull of a set,” *Uspekhi Matematicheskikh Nauk*, vol. 19, no. 6, pp. 139–145, 1964.
- [22] G. Schwarz *et al.*, “Estimating the dimension of a model,” *The annals of statistics*, vol. 6, no. 2, pp. 461–464, 1978.
- [23] G. Schreiber, A. Stemmer, and R. Bischoff, “The fast research interface for the KUKA lightweight robot,” in *Proc. of the IEEE Workshop on Innovative Robot Control Architectures for Demanding (Research) Applications – How to Modify and Enhance Commercial Controllers (ICRA 2010)*, IEEE, 2010.